IMMUNOLOGY

# The proliferation of human mucosal-associated invariant T cells requires a MYC-SLC7A5-glycolysis metabolic axis

**Nidhi Kedia-Mehta[1]†, Marta M. Pisarska[1,2]†, Christina Rollings[3], Chloe O'Neill[2], Conor De Barra[2], Cathriona Foley[4], Nicole A. W. Wood[1,2], Neil Wrigley-Kelly[5,6], Natacha Veerapen[7], Gurdyal Besra[7], Ronan Bergin[2], Nicholas Jones[8], Donal O'Shea[2,5,6], Linda V. Sinclair[3]*, Andrew E. Hogan[1,2]***



**Mucosal-associated invariant T (MAIT) cells are an abundant population of innate T cells that recognize bacterial ligands and play a key role in host protection against bacterial and viral pathogens. Upon activation, MAIT cells undergo proliferative expansion and increase their production of effector molecules such as cytokines. In this study, we found that both mRNA and protein abundance of the key metabolism regulator and transcription factor MYC was increased in stimulated MAIT cells. Using quantitative mass spectrometry, we identified the activation of two MYC-controlled metabolic pathways, amino acid transport and glycolysis, both of which were necessary for MAIT cell proliferation. Last, we showed that MAIT cells isolated from people with obesity showed decreased *MYC* mRNA abundance upon activation, which was associated with defective MAIT cell proliferation and functional responses. Collectively, our data uncover the importance of MYC-regulated metabolism for MAIT cell proliferation and provide additional insight into the molecular basis for the functional defects of MAIT cells in obesity.**

## INTRODUCTION

Mucosal-associated invariant T (MAIT) cells are a population of non–major histocompatibility complex (MHC)–restricted T cells that are important in the immune defense against bacterial and viral infections (*1*–*5*). In addition to their abundance (2 to 10% of total T cells) in peripheral blood, MAIT cells are relatively abundant across a range of human tissues, including adipose, gut, and liver, where they can account for up to 50% of all T cells (*6*). MAIT cells are early responding T cells that are capable of producing multiple cytokines rapidly upon activation such as interferon-γ (IFN-γ), tumor necrosis factor, and interleukin-17 (IL-17) (*1*, *7*). Because of their robust production of effector molecules, MAIT cells have been implicated in both host protection [against pathogens (*6*) and cancer cells (*8*)] and tissue repair (*9*–*11*). MAIT cells are activated when their invariant T cell receptor (TCR) recognizes bacterial derivatives presented on the MHC-like molecule MR1 (*5*, *7*). MAIT cells can also be activated in a TCR-independent manner through cytokine stimulation (*10*, *12*). Altered MAIT cell cytokine profiles have been reported in several diseases, including obesity, arthritis, and viral infection (*13*–*18*).

One key functional response of MAIT cells is their ability to proliferate rapidly upon activation, which has been demonstrated both in vitro and in vivo (*19*–*21*). Increased immune signal–driven proliferation relies on metabolic reprogramming to provide large amounts of energy and biosynthetic intermediates needed to support the rapid generation of new cells (*22*). In conventional T cells, metabolic reprogramming in response to activation is controlled by the transcription factor MYC, which acts as a master metabolic regulator (*23*). MYC expression is rapidly induced after TCR stimulation and is sustained by amino acid availability and IL-2 signaling (*24*–*26*). In particular, the expression of the amino acid transporter SLC7A5, which is under the control of MYC, forms a feed-forward loop in which amino acid transport through SLC7A5 sustains MYC protein expression (*24*). Whether MYC acts as a metabolic regulator in MAIT cells is currently unknown. Although it is known that MAIT cell cytokine production is dependent on glycolytic metabolism, it is unclear what regulates and fuels MAIT cell proliferation (*27*). To address these unknowns, we have interrogated the molecular and metabolic requirements for MAIT cell proliferation. In addition, defective natural killer (NK) and MAIT cell metabolism and defective cellular responses are present in people with obesity (PWO), which may translate to elevated incidences of comorbid diseases (*27*–*29*). However, the impact of obesity on important metabolic regulators such as MYC is not clearly understood and remains to be elucidated.

Using quantitative mass spectrometry (MS), we identified a robust up-regulation of MYC expression and MYC-controlled metabolic pathways in stimulated MAIT cells. We showed that MYC-regulated metabolic pathways (including amino acid transport and glycolysis) are essential for human MAIT cell proliferation. Last, we showed that obesity is associated with defective MAIT cell proliferation because of a defective MYC-SLC7A5-glycolysis metabolic axis. Collectively, our data demonstrated that MYC acts as a metabolic regulator in TCR and cytokine-stimulated MAIT cells and that this is essential for proliferation and provide further molecular insight into obesity-related defects in human MAIT cells.

[1]Kathleen Lonsdale Institute for Human Health Research, Maynooth University, Maynooth, Co Kildare, Ireland. [2]National Children's Research Centre, Dublin 12, Ireland. [3]Division of Cell Signaling and Immunology, School of Life Sciences, University of Dundee, Dundee, UK. [4]Department of Biological Sciences, Munster Technological University, Cork, Ireland. [5]St. Vincent's University Hospital, Dublin 4, Ireland. [6]University College Dublin, Dublin 4, Ireland. [7]School of Biosciences, University of Birmingham, Birmingham, UK. [8]Institute of Life Science, Swansea University Medical School, Swansea, UK.
†These authors contributed equally to this work.
*Corresponding author. Email: andrew.e.hogan@mu.ie (A.E.H.); l.v.sinclair@dundee.ac.uk (L.V.S.)

## RESULTS

### MAIT cells remodel their proteomes upon TCR activation

To investigate the major pathways regulating MAIT cell activation, we performed quantitative MS on MAIT cells expanded by treatment with IL-2 ($MAIT^{IL\text{-}2}$ cells) before and after TCR stimulation (anti-TCR/CD28 and IL-12/IL-18; $MAIT^{STIM}$). We identified 5740 proteins in both IL-2–maintained and IL-2–stimulated MAIT cells and have estimated the absolute protein copy number per cell using the proteomic ruler method that uses the MS signal of histones as an internal standard (data file S1) (*30*). Only a small proportion of highly abundant proteins accounts for most cellular mass in conventional effector T cells (*24*, *31*, *32*); in human MAIT cells, we found that expression of eight proteins (fig. S1) contributes 25% of the total mass, and expression abundance of about 350 proteins

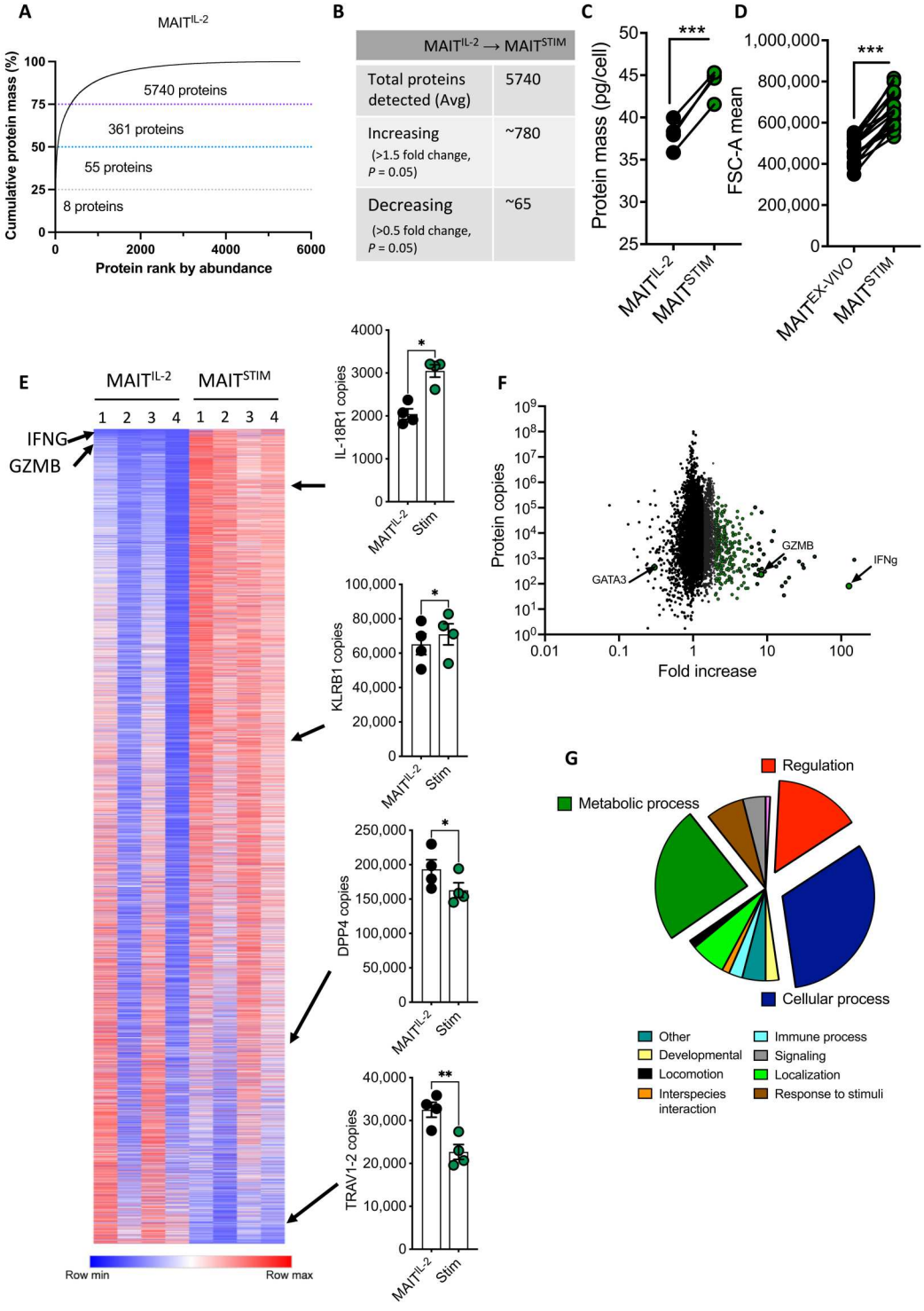


**Fig. 1. Remodeling of MAIT cell proteome after activation.** (**A**) Proteins from IL-2–expanded MAIT ($MAIT^{IL\text{-}2}$) cells were ranked by mass contribution, and the mean cumulative protein mass was plotted against protein rank ($n = 4$). (**B**) Table outlining the total number of proteins detected in $MAIT^{IL\text{-}2}$ cells and their change upon stimulation [$MAIT^{STIM}$; 18 hours with anti-CD3/CD28 beads and IL-12 and IL-18 (50 ng/ml)] using quantitative proteomics ($n = 4$ per group). (**C**) Protein mass in $MAIT^{IL\text{-}2}$ or $MAIT^{STIM}$ ($n = 4$). (**D**) Scatterplot showing ex vivo MAIT cell size (forward scatter) basally or stimulated (as above) ($n = 15$). (**E**) Heatmap of the proteome of $MAIT^{IL\text{-}2}$ and $MAIT^{STIM}$ cells (as above) ($n = 4$ per group). Relative protein abundance is graded from blue (low) to red (high) per row. Key MAIT cell proteins (IL-18R1, KLRB1, DPPIV, and TRAV1-2) are represented in scatter graphs, and their positions in the heatmap are denoted by arrows ($n = 4$/group). (**F**) Scatterplot displaying the copy numbers against fold change of the $MAIT^{STIM}$ cell proteome compared with $MAIT^{IL\text{-}2}$ (green circles represent proteins increased more than 1.5-fold over $MAIT^{IL\text{-}2}$ cells). (**G**) Pie chart showing proportional pathway analysis based on the $MAIT^{STIM}$ cell proteome (analysis performed with Panther; raw data in data file S1). $^*P < 0.05$, $^{**}P < 0.01$, and $^{***}P < 0.001$.

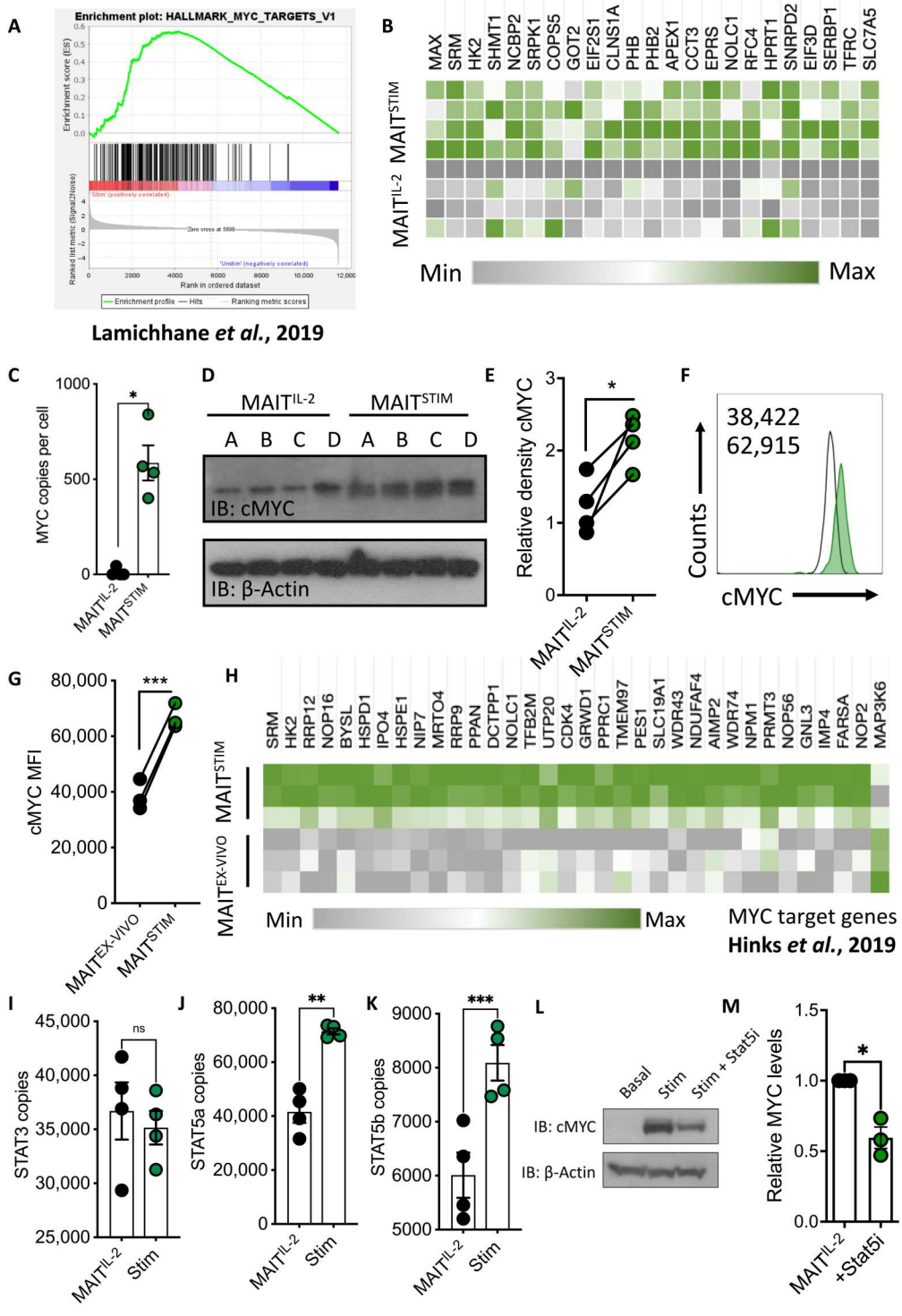


**Fig. 2. Activation of MYC and its target pathways in MAIT cells.** (**A**) GSEA plot showing the increase in MYC target gene expression in activated MAIT cells. Data extrapolated from previously published RNA sequence dataset (*10*) on ex vivo MAIT cells stimulated through TCR. (**B**) Heatmap displaying expression amounts of MYC target in basal ($MAIT^{IL\text{-}2}$) or stimulated [$MAIT^{STIM}$; 18 hours of anti-CD3/CD28 beads + IL-12 and IL-18 (50 ng/ml)] cells as determined by quantitative proteomics ($n = 4$ per group). Relative protein abundance is graded from gray (low) to green (high) per row. (**C**) Proteomic determination of MYC protein expressed as copies per cell from basal ($MAIT^{IL\text{-}2}$) or stimulated ($MAIT^{STIM}$) cells ($n = 4$ per group) (note that identification is based on a single peptide hit). (**D** and **E**) Western blot and densitometry displaying MYC expression in $MAIT^{IL\text{-}2}$ or stimulated (as above) $MAIT^{STIM}$ cells ($n = 4$). (**F** and **G**) Representative flow cytometry histogram (F) [mean fluorescence intensity (MFI) values are shown within histogram] and MFI values (G) of MYC expression in $MAIT^{EX\text{-}VIVO}$ cells (black) or $MAIT^{STIM}$ (green) ($n = 4$). (**H**) Heatmap displaying MYC target genes in $MAIT^{EX\text{-}VIVO}$ cells with or without TCR stimulation. Data extrapolated from previously published RNA sequence dataset (*11*). (**I** to **K**) Scatterplots showing STAT3, STAT5a, and STAT5b protein levels expressed as copies per cell from basal ($MAIT^{IL\text{-}2}$) or stimulated ($MAIT^{STIM}$) cells ($n = 4$ per group). (**L** and **M**) Western blot and densitometry displaying MYC expression in $MAIT^{IL\text{-}2}$ or $MAIT^{STIM}$ cells in the absence or presence of a STAT5i ($n = 3$). $^{*}P < 0.05$, $^{**}P < 0.01$, and $^{***}P < 0.001$. ns, not significant.

accounts for 75% of the total cellular mass (Fig. 1A). Upon TCR activation, we observed remodeling of the $MAIT^{IL\text{-}2}$ cell proteome (Fig. 1B), which was accompanied by an increase in total protein mass and cell size (Fig. 1, C and D). The expression of the most abundant proteins did not change after stimulation and remained proportional to the amounts expressed basally in $MAIT^{IL\text{-}2}$ cells (fig. S1). Signature effector proteins such as IFNG and granzyme B (GRZB) were among the most highly increased proteins upon stimulation (Fig. 1, E and F). We were also able to detect many proteins associated with a core MAIT cell signature, including IL-18R1 (IL-18 receptor 1; which strongly increased expression in response to stimulation), KLRB1 (moderate increase), DPPIV (moderately decreased), and TRAV1-2 (expression was decreased upon stimulation) (Fig. 1E). In total, 780 proteins were increased more than 1.5-

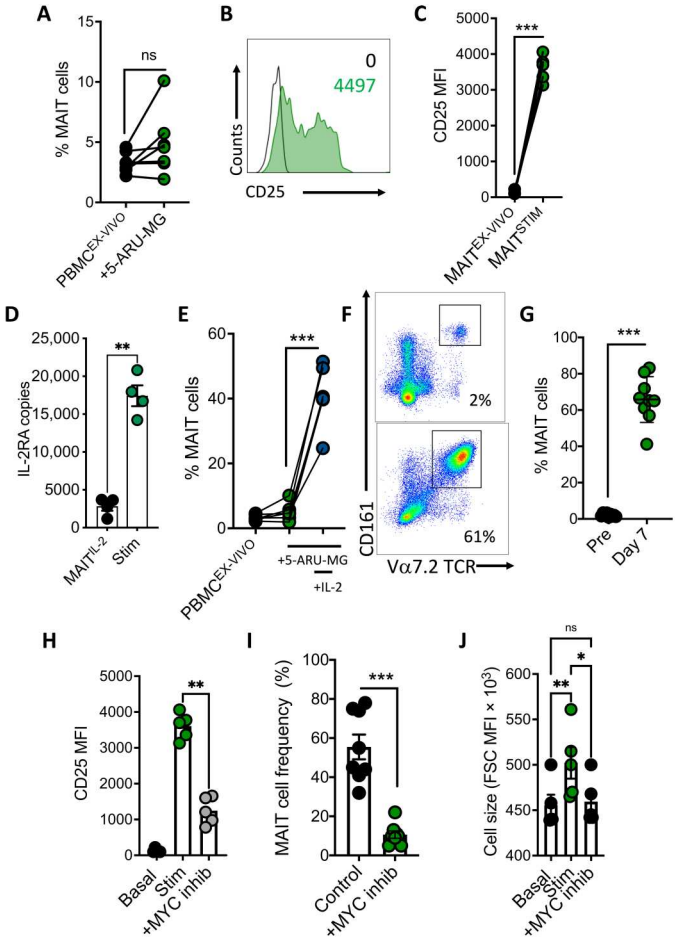


**Fig. 3. IL-2–driven proliferation of MAIT cells is dependent on MYC.** (**A**) The frequency of MAIT cells (as a percentage of total T cells) after stimulation of PBMCs ($1 \times 10^6$) with antigenic stimulation (cognate antigen 5-ARU and methylglyoxal) for 7 days ($n = 6$). (**B** and **C**) Representative flow cytometry histogram and scatterplot showing CD25 (IL-2RA) expression on $MAIT^{EX\text{-}VIVO}$ or stimulated through the TCR using anti-CD3/CD28 beads/IL-12 and IL18 ($MAIT^{STIM}$) for 18 hours ($n = 9$). (**D**) CD25 protein expressed as copies per cell from $MAIT^{IL\text{-}2}$ cells basally or $MAIT^{STIM}$ ($n = 4$). (**E**) Graph demonstrating frequency of MAIT cells (represented as percentage of T cells) after stimulation with 5-ARU (1 μg/ml) and methylglyoxal (100 μM) in the absence or presence of IL-2 (33.3 ng/ml) for 7 days ($n = 5$). (**F** and **G**) Representative flow cytometry dot plot and scatterplot showing MAIT cell frequencies after 7 days of stimulation with 5-ARU, methylglyoxal, and IL-2 ($n = 10$). (**H**) MFI of CD25 expression on MAIT cells after 18 hours of stimulation [as in (C) in the absence or presence of the MYC inhibitor (10074-G5, 10 μM) ($n = 5$). (**I**) $MAIT^{IL\text{-}2}$ cell frequency after 7 days of expansion [as in (E)] in the absence of presence of the MYC inhibitor 10074-G5 (10 μM) ($n = 8$). (**J**) Forward scatter MFI of MAIT cells after stimulation [as in (C)] in the absence of presence of the MYC inhibitor 10074-G5 ($n = 5$). *$P < 0.05$, **$P < 0.01$, and ***$P < 0.001$.

fold upon activation (Fig. 1, B and F). Pathway analysis highlighted that the increased proteins were enriched in multiple processes and included a large proportion involved in governing cellular metabolism (Fig. 1G).

## MAIT cells up-regulate expression of the transcription factor MYC and its downstream target pathways upon activation

In silico pathway analysis of a previously published RNA sequencing dataset (*10*) revealed that MAIT cells activated ex vivo ($MAIT^{EX\text{-}VIVO}$ cells) have a strong MYC signature, as determined by the Hallmark gene set enrichment analysis (GSEA) (Fig. 2A and fig. S2). In our activated human $MAIT^{IL\text{-}2}$ proteomic dataset, we also found increased MYC expression and its target proteins (Fig. 2, B and C). Using alternative methods to measure MYC expression, we show that MYC protein expression is increased in $MAIT^{IL\text{-}2}$ cells stimulated through their TCRs (Fig. 2, D and E). We next interrogated MYC expression in TCR-stimulated $MAIT^{EX\text{-}VIVO}$ cells (Fig. 2, F and G). Together, these data show that MYC is increased in response to TCR stimulation in both $MAIT^{EX\text{-}VIVO}$– and $MAIT^{IL\text{-}2}$–expanded cells. To further support the increased expression of MYC targets in activated MAIT cells, we analyzed another published RNA sequencing dataset (*11*) and once again saw increased MYC target gene expression in activated MAIT cells (Fig. 2H and fig. S3). TCR activation induces MYC expression in conventional $CD8^+$ T cells (*26*). Furthermore, MYC expression is maintained by IL-2 through the activation of JAK/STAT (Janus kinase/signal transducer and activator of transcription) signaling pathways (*26*). With this in mind, we interrogated the upstream signals required for MYC activation in MAIT cells. We compared the ability of TCR stimulation and the cytokines IL-2, IL-12, and IL-18 to induce MYC expression in $MAIT^{IL\text{-}2}$ cells, with TCR triggering induced the strongest MYC expression (fig. S4) (*26*). Analysis of the $MAIT^{IL\text{-}2}$ proteomic data showed that, upon activation, MAIT cells had increased abundance of STAT5 but not STAT3 (Fig. 2, I to K). Furthermore, inhibition of STAT5 activation reduced MYC expression in TCR-activated MAIT cells (Fig. 2, L and M).

## MAIT cell proliferation is dependent on MYC

MAIT cells can readily proliferate upon TCR activation with a cognate antigen or bacterial infection (*20*, *21*). To build on these observations, we investigated the ability of $MAIT^{EX\text{-}VIVO}$ cells to proliferate in vitro after stimulation with the riboflavin metabolite 5-ARU, which is further processed into the MAIT cell cognate antigen 5-OP-RU, resulting in a full antigenic stimulation through the TCR. $MAIT^{EX\text{-}VIVO}$ cells activated with antigenic stimulation failed to proliferate despite increased expression of activation markers such the IL-2Rα chain, CD25 (Fig. 3, A to C). Increased expression of CD25 was also noted on $MAIT^{IL\text{-}2}$ cells after TCR bead stimulation (Fig. 3D). IL-2 is a driver of T cell growth and proliferation (*33*), so we investigated whether the addition of IL-2 alongside antigenic stimulation could drive $MAIT^{EX\text{-}VIVO}$ cell proliferation. Addition of IL-2 resulted in significant MAIT cell growth and proliferation in combination with antigenic stimulation (Fig. 3, E to G). MYC expression is required for conventional T cell blasting and proliferation in response to TCR signaling (*23*, *24*). Many of the transcriptional programs driven by MYC are dependent on dimerization with MAX (*34*). The MYC inhibitor 10074-G5 blocks the binding of MAX to MYC and thereby inhibits transcriptional activity (*35*). Using this inhibitor, we saw that the increase in cell size and CD25 expression in MAIT cells after TCR simulation was dependent on MYC activity (Fig. 3, H and I). Furthermore, MYC activity was required for MAIT cell proliferation in response to TCR and IL-2 (Fig. 3J and fig. S5).

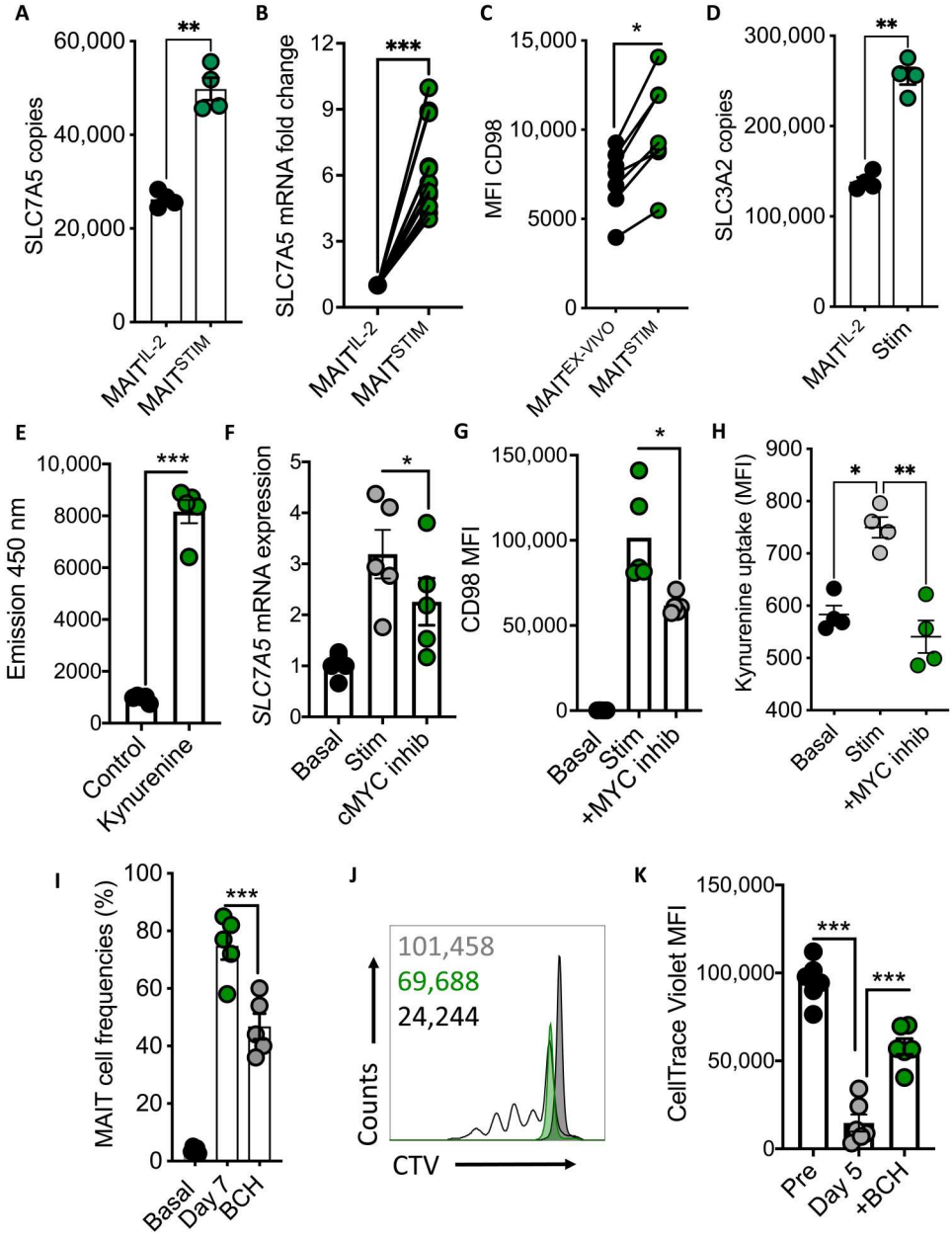


**Fig. 4. SLC7A5 facilitates MAIT cell proliferation and is dependent on MYC.** (**A**) Mean protein copy number per cell of SLC7A5 in MAIT$^{IL-2}$ cells and in cells stimulated for 18 hours (MAIT$^{STIM}$; anti-CD3/CD28 beads/IL-12 and IL18) ($n = 4$). (**B**) Scatterplot showing SLC7A5 mRNA expression in MAIT$^{IL-2}$ cells or MAIT$^{STIM}$ [as in (A)] ($n = 12$). (**C**) Flow cytometry MFI data of CD98 expression on ex vivo MAIT cells or stimulated for 18 hours [as in (A)] ($n = 7$). (**D**) Mean protein copy number per cell of SLC3A52 in basal or stimulated MAIT$^{IL-2}$ cells ($n = 4$ per group). (**E**) Flow cytometry data of uptake of kynurenine into ex vivo MAIT cells ($n = 5$). (**F**) SLC7A5 mRNA expression in MAIT$^{IL-2}$ cells and MAIT$^{STIM}$ [as in (A)] in the absence or presence of the MYC-specific inhibitor 10074-G5 ($n = 5$). (**G**) Flow cytometry MFI expression of CD98 on ex vivo MAIT cells after stimulation [as in (A)] in the absence or presence of the MYC-specific inhibitor 10074-G5 (10 μM) ($n = 5$). (**H**) Flow cytometry data of uptake of kynurenine into MAIT$^{IL-2}$ cells stimulated for 18 hours (anti-CD3/CD28 beads/IL-12 and IL18) in the absence or presence of the MYC inhibitor iBET 762 ($n = 4$). (**I**) The frequency of MAIT cells after 7 days of expansion with 5-ARU (1 μg/ml) and methylglyoxal (100 μM) in the absence or presence of IL-2 (33.3 ng/ml) and in the absence of presence of the SLC7A5 inhibitor BCH ($n = 5$). (**J** and **K**) Representative flow cytometry histogram and scatterplot showing CellTrace Violet (CTV) MFI in MAIT cells after 5 days of stimulation [as in (G)] in the absence of presence of BCH ($n = 7$). *$P < 0.05$, **$P < 0.01$, and ***$P < 0.001$.

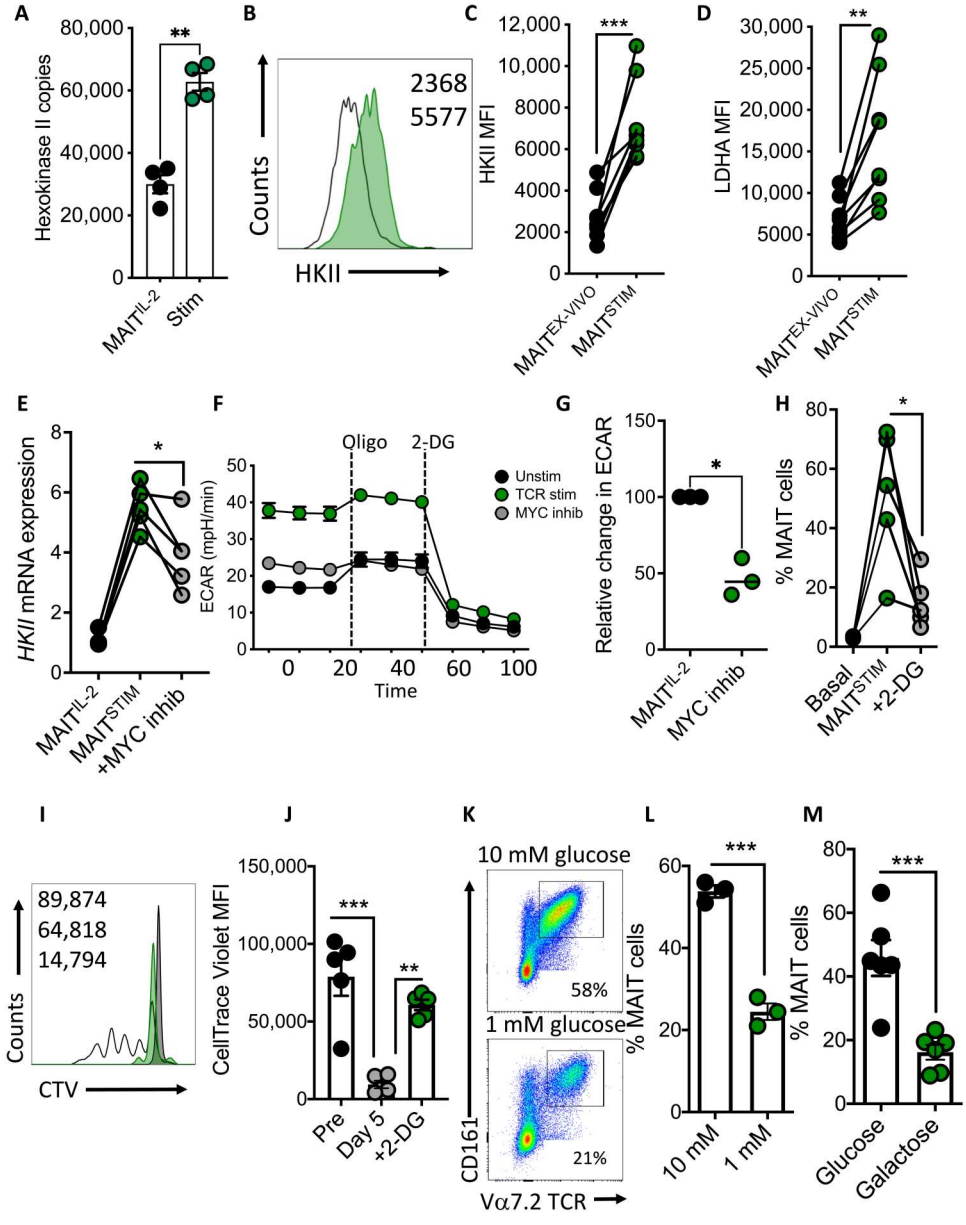


**Fig. 5. Glucose metabolism facilitates MAIT cell proliferation and is dependent on MYC.** (**A**) Mean protein copy number per cell of hexokinase-II (HKII) in $MAIT^{IL\text{-}2}$ and in $MAIT^{IL\text{-}2\ +\ STIM}$ (stimulated for 18 hours with anti-CD3/CD28 beads and IL-18 (50 ng/ml) ($n = 4$). (**B** and **C**) Representative flow cytometry histogram and MFI data of HKII in $MAIT^{EX\text{-}VIVO}$ cells basally or stimulated [18 hours with anti-CD3/CD28 beads and IL-18 (50 ng/ml); $MAIT^{STIM}$] ($n = 8$). (**D**) Flow cytometry MFI data of lactate dehydrogenase A (LDHA) expression in $MAIT^{EX\text{-}VIVO}$ and $MAIT^{STIM}$ cells [as in (C)] ($n = 8$). (**E**) HKII mRNA expression in $MAIT^{IL\text{-}2}$ and in $MAIT^{IL\text{-}2\ +\ STIM}$ cells [as in (A)] in the absence or presence of the MYC-specific inhibitor 10074-G5 ($n = 5$). (**F** and **G**) Representative Seahorse Analyzer trace and scatterplot detailing the ECAR rates of $MAIT^{IL\text{-}2}$ cells stimulated for 18 hours (anti-CD3/CD28 beads/IL-12 and IL18) in the absence or presence of the MYC inhibitor iBET 762 ($n = 4$). (**H**) The frequency of MAIT cells after 7 days of expansion from PBMCs ($1 \times 10^6$) using the cognate antigen 5-ARU (1 μg/ml), methylglyoxal (100 μM), and IL-2 (33.3 ng/ml) in the absence or presence of the glycolysis inhibitor 2-DG (2 mM) ($n = 5$). (**I** and **J**) Representative flow cytometry histogram and scatterplot showing CellTrace Violet (CTV) MFI in MAIT cells after 5 days of stimulation in the absence of presence of 2-DG ($n = 5$). (**K** and **L**) Representative flow cytometry dot plot and MAIT cell frequencies after 7 days of stimulation in media containing either 10 or 1 mM glucose ($n = 3$). (**M**) MAIT cell frequencies after 7 days of stimulation in media containing either 10 mM glucose or 10 mM galactose ($n = 6$). $^*P < 0.05$, $^{**}P < 0.01$, and $^{***}P < 0.001$.

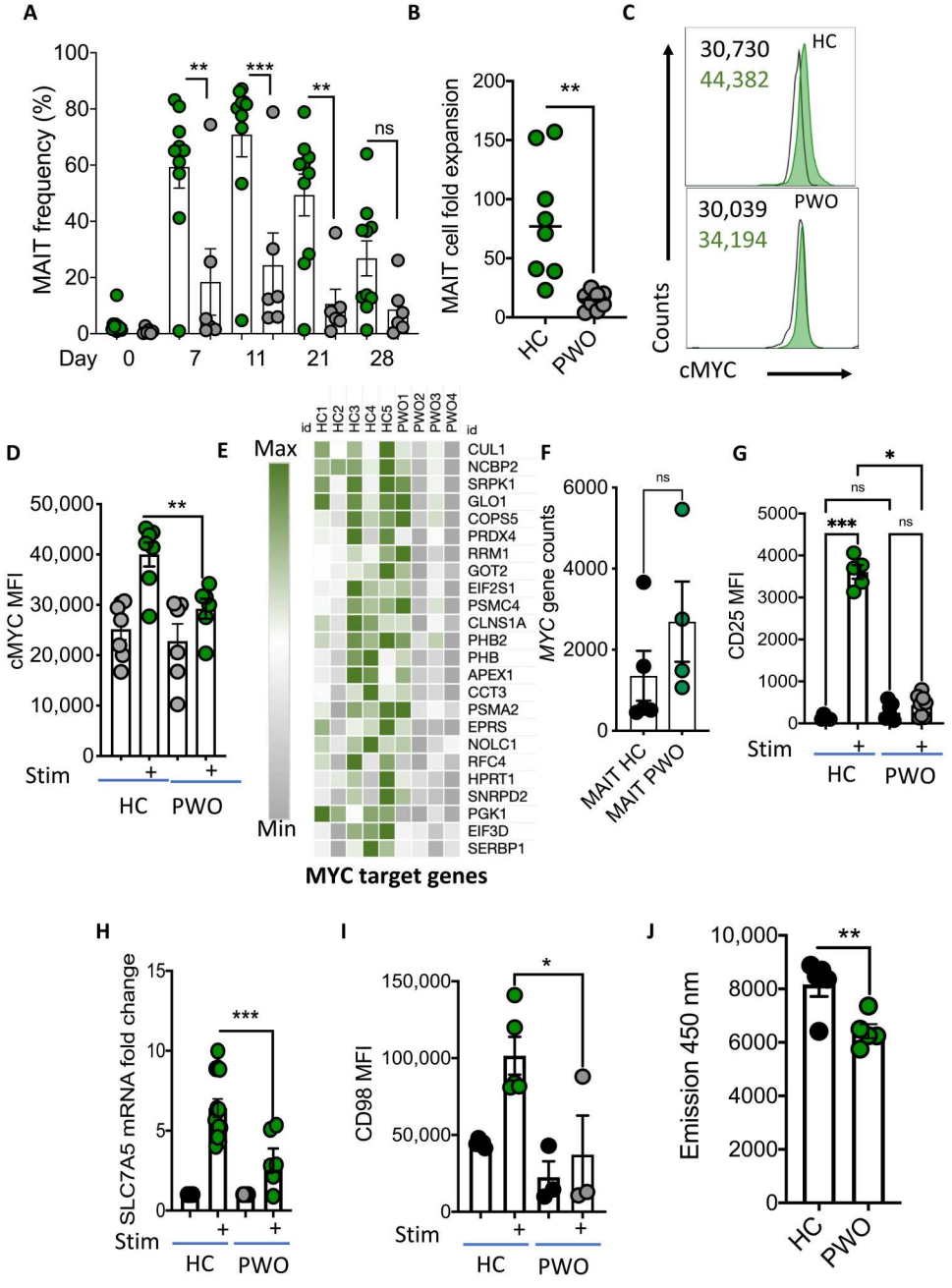


**Fig. 6. MYC is defective in obesity, resulting in diminished MAIT cell proliferation.** (**A**) The frequency of MAIT cells after 0 to 28 days of expansion after 18-hour stimulation with 5-ARU (1 μg/ml), methylglyoxal (100 μM), and maintenance in IL-2 (33.3 ng/ml) in either healthy controls (green circles) or people with obesity (PWO) (gray circles) ($n = 10$ per group). (**B**) Fold expansion of MAIT cells from healthy controls or PWO after 7 days of stimulation [with 5-ARU (1 μg/ml), methylglyoxal (100 μM), and IL-2 (33.3 ng/ml)] ($n = 8$). (**C** and **D**) Representative flow cytometry histogram (C) and MFI data (D) of MYC expression in ex vivo MAIT cells from healthy controls [top (C)] or PWO [bottom (C)] stimulated with anti-CD3/CD28 beads and IL-18 (50 ng/ml) for 18 hours ($n = 6$ or 7 per group). (**E**) Scatter graph showing MYC gene counts [extrapolated from published RNA sequencing dataset (*27*)] in ex vivo MAIT cells from healthy controls or PWO ($n = 4$ or 5 per group). (**F**) Heatmap displaying MYC target genes in ex vivo MAIT cells from healthy controls or PWO ($n = 4$ or 5 per group). (**G**) CD25 expression (MFI) on ex vivo MAIT cells or stimulated MAIT cells [as in (C)] from either healthy controls or PWO ($n = 5$ to 8 per group). (**H**) mRNA expression of *Slc7a5* in $MAIT^{IL\text{-}2}$ cells or $MAIT^{IL\text{-}2}$ stimulated [as in (C)] from either healthy controls or PWO ($n = 6$ to 10 per group). (**I**) Scatterplot showing CD98 expression (MFI) on ex vivo MAIT cells basally or stimulated [as in (C)] from either healthy controls or PWO ($n = 3$ or 4 per group). (**J**) Scatterplot showing kynurenine uptake into MAIT cells from either healthy controls or PWO ($n = 5$ per group). $^*P < 0.05$, $^{**}P < 0.01$, and $^{***}P < 0.001$.

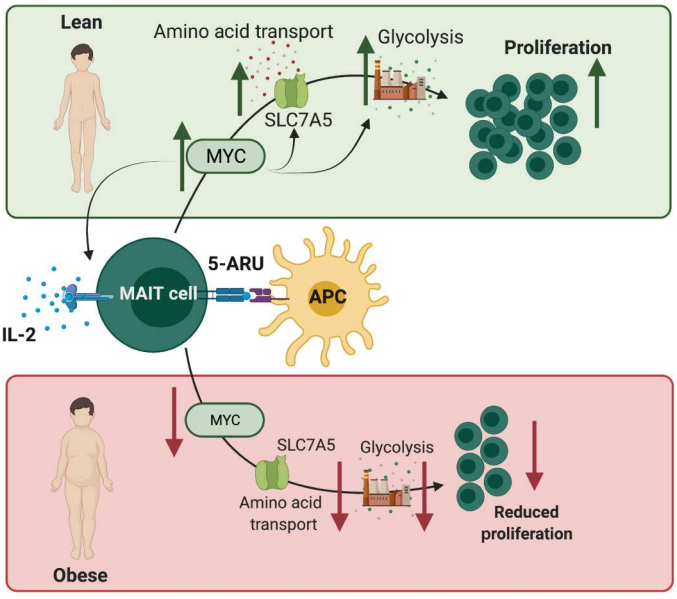


**Fig. 7. Working model.** Schematic outlining the proposed working model. (**Top**) A MYC-SLC7A5-glycolysis axis in activated MAIT cells. (**Bottom**) The impact of obesity on the proposed MYC-SLC7A5-glycolysis axis in activated MAIT cells.

### The MYC-controlled amino acid transporter SLC7A5 is required for MAIT cell proliferation

Proliferation is a metabolically intense process, requiring large amounts of energy and de novo generation of biosynthetic intermediates; so we next investigated metabolic processes under the control of MYC. In conventional murine T cells, TCR-driven expression of MYC induces the expression of critically important amino acid transporters, including SLC7A5 (*24*). SLC7A5 and its heavy chain chaperone, CD98 (SLC3A2), form the heterodimeric large neutral amino acid transporter (LAT-1). Interrogation of the MAIT cell proteomes shows that *SLC7A5* expression increases from 25,000 copies per cell in $MAIT^{IL\text{-}2}$ cells to 50,000 copies per cell in $MAIT^{IL\text{-}2\ +\ STIM}$ cells (Fig. 4A), which correlates with increased mRNA expression in $MAIT^{IL\text{-}2\ +\ STIM}$ compared with $MAIT^{IL\text{-}2}$ cells (Fig. 4B). We also noted increased expression of CD98/SLC3A2 (Fig. 4, C and D). Together, these data show that that, upon TCR activation, both $MAIT^{EX\text{-}VIVO}$ and $MAIT^{IL\text{-}2}$ cells increase the expression of SLC7A5 protein, *SLC7A5* mRNA, and CD98 surface expression (Fig. 4, A to C). Using a flow cytometry–based assay, uptake of kynurenine, a fluorescent SLC7A5 substrate, was monitored in MAIT cells. $MAIT^{EX\text{-}VIVO}$ cells exhibited low kynurenine uptake; however, upon TCR/cytokine stimulation, $MAIT^{EX\text{-}VIVO}$ cells rapidly increase transport through SLC7A5 (Fig. 4E). From our proteomic analysis, we also noted that, upon activation, MAIT cells increase expression of several other amino acid transporters, including SLC1A5, SLC7A1, and SLC38A1, which are also controlled by MYC (fig. S6) (*24*). We used MYC inhibitors to investigate whether the TCR/cytokine-driven increase in LAT-1 expression was dependent on MYC activity. Inhibition of MYC resulted in reduced *SLC7A5* mRNA expression and reduced CD98 expression in activated MAIT cells (Fig. 4, F and G). Furthermore, inhibition of MYC reduced the uptake of the SLC7A5 substrate kynurenine by activated MAIT cells (Fig. 4H). Next, we investigated whether loss of amino acid transport via LAT-1 affected MAIT cell proliferation. Using the competitive substrate 2-amino-bicyclo-(2,2,1)-heptane-2-carboxylic acid (BCH) to block LAT-1 activity, we showed that MAIT cell proliferation is limited when uptake through LAT-1 is blocked. Therefore, SLC7A5 activity during TCR/IL-2 activation is required for $MAIT^{EX\text{-}VIVO}$ cell proliferation (Fig. 4, I to K).

### Glucose metabolism supports MAIT cell proliferation

MYC has been highlighted as a master regulator of glycolysis (*23*, *24*), and, therefore, we investigated whether glucose metabolism was required for MAIT cell proliferation. We have reported that MAIT cells had increased glycolytic metabolism upon activation (*27*); here, we noted increased expression of the glycolytic enzymes [hexokinase-II (HKII) and lactate dehydrogenase (LDH)] in both $MAIT^{EX\text{-}VIVO}$ and $MAIT^{IL\text{-}2}$ cells after TCR stimulation (Fig. 5, A to D). Inhibition of MYC resulted in diminished *HKII* mRNA expression in activated $MAIT^{EX\text{-}VIVO}$ cells (Fig. 5E). We also showed that inhibition of MYC limited the rates of glycolytic metabolism in TCR-activated MAIT cells (Fig. 5, F and G). To investigate whether glucose metabolism is required for MAIT cell proliferation, we treated MAIT cells with the glycolytic inhibitor 2-deoxyglucose (2-DG). MAIT cell proliferation was inhibited when treated with 2-DG (Fig. 5, H to J). Limiting the glucose availability in the culture media from 10 to 1 mM reduced MAIT cell proliferation (Fig. 5, K and L). Last, replacing the carbon source in the culture media from glucose to galactose [which slows the rates of glycolysis (*36*)] resulted in reduced MAIT cell proliferation (Fig. 5M).

### MAIT cells from PWO display blunted MYC expression and fail to proliferate

MAIT cell frequencies and cytokine production are altered in PWO (*14*, *37*, *38*). We investigated the proliferative capacity of MAIT cells from PWO in response to a combination of antigenic (5-ARU-MG) and cytokine (IL-2) stimulation. MAIT cells from PWO displayed defective proliferation in response to immune stimulation when compared with healthy controls (Fig. 6, A and B, and fig. S7). These data provided further evidence that MAIT cells are functionally affected by obesity. Having highlighted the critical importance of MYC for MAIT cell proliferative responses, we assessed MYC expression in cohorts of PWO and healthy controls and found impaired induction of MYC expression in $MAIT^{EX\text{-}VIVO}$ cells in response to immune activation from PWO (Fig. 6, C and D). Targeted analysis of a previously published RNA sequencing dataset on MAIT cells isolated from PWO and healthy controls (*27*) showed reduced expression of MYC target gene expression in MAIT cells from PWO (Fig. 6E). *MYC* RNA expression in these same individuals was not reduced (Fig. 6F), indicating that signaling downstream of immune activation to drive expression of MYC RNA was not impaired. Because CD25 surface protein expression was reduced with MYC inhibition (Fig. 3H), we measured CD25 expression on MAIT cells from PWO and found diminished CD25 levels in response to TCR and cytokine activation (Fig. 6G). Having identified that SLC7A5, a direct transcriptional target of MYC, is critical for MAIT cell proliferation in response to immune stimulation, we measured SLC7A5 expression on MAIT cells from PWO. We demonstrated that, upon activation, MAIT cells from PWO express significantly less *SLC7A5* mRNA and CD98, resulting in reduced

amino acid transport, a process necessary for proliferation (Fig. 6, H to J).

## DISCUSSION

MAIT cells are a subset of unconventional T cells that are abundant in human blood and tissues, including liver and adipose tissue (*6*, *39*). MAIT cells are capable of responding rapidly to stimulation by producing cytokines and lytic molecules, as well as proliferating (*6*). Because of their potent effector functions and abundance, MAIT cells have been shown to play an important role in the host defense against pathogens and malignancies (*1*, *8*) and are of interest as a potential immunotherapeutic agent (*21*, *40*). However, the molecular regulation of MAIT cell effector functions is still emerging. In the current study, we demonstrated that MAIT cell proliferation is dependent on the transcription factor MYC. We showed that, upon activation, MAIT cells had a greater abundance of MYC target proteins, including SLC7A5 and HKII, which are both integral to key processes required for MAIT cell proliferation. Last, we showed that MYC expression and targets under the control of MYC are defective in PWO, underpinning diminished MAIT cell proliferation (Fig. 7). These observations suggest a mechanism that may increase host susceptibility to infection and malignancies.

Quantitative MS allows a high-dimensional analysis of the proteome and activation-induced remodeling (*24*–*26*). Using this approach, we were able to identify 5740 proteins in both resting IL-2–expanded MAIT cells and stimulated IL-2–expanded MAIT cells, similar to previously published datasets (*41*, *42*). TCR and cytokine stimulation were associated with the remodeling of the MAIT cell proteome and were associated with significant increases in protein content and cell size. Pathway analysis of our proteomic dataset and previously published RNA sequencing datasets revealed the MYC pathway as one of the most up-regulated in MAIT cells. MYC is a critically important transcription factor in conventional T cells and acts as a metabolic master regulator (*23*, *24*, *26*). Experiments using high-dimensional quantitative MS on $CD4^+$ and $CD8^+$ T cells from wild-type and MYC-deficient mice reveal how MYC controls TCR-driven cell growth and metabolism (*23*, *24*). We showed that MYC is a critical regulator of human MAIT cell proliferation.

MAIT cell proliferation was triggered in a two-step process, where activation with 5-ARU-MG, which forms the MAIT cell cognate antigen 5-OP-RU, did not drive MAIT cell proliferation but did trigger the expression of the high-affinity IL-2R CD25. Subsequent addition of IL-2 drove MAIT cell proliferation. A similar two-step process occurs in conventional $CD8^+$ T cells, in which IL-2 is not required for the initiation of proliferation but required for sustaining proliferation (*43*). We also demonstrated that increased expression of CD25 by activated MAIT cells was dependent on MYC, which aligns with previous reports demonstrating that, in MYC-deficient conventional T cells, the expression of CD25 does not increase upon stimulation (*24*).

MYC signaling is also essential for the up-regulation of amino acid transporters on T cells, including SLC7A5 (*24*). We have previously reported that MAIT cells express SLC7A5 (*27*) and demonstrated here that inhibition of MYC results in diminished SLC7A5 and CD98 expression as well as reduced transport of the SLC7A5 substrate kynurenine by activated MAIT cells. Amino acid transport by SLC7A5/CD98 is critical for sustained expression of MYC, suggesting a positive feed-forward loop (*24*). Using the SLC7A5 inhibitor BCH, we showed that amino acid transport through SLC7A5 is needed for MAIT cell proliferation. This highlights the presence of a MYC-SLC7A5 axis present in activated MAIT cells, similar to that identified in conventional T cells.

MYC also directs a glycolytic metabolism program in conventional T cells (*23*, *24*, *26*), which is important for T cell growth, activation, and effector functions (*44*). Glycolytic metabolism is required for MAIT cell cytokine and lytic molecule production (*27*, *37*, *45*), but the factors regulating MAIT cell metabolism and the requirements for MAIT cell proliferation are unknown. Here, we show that MAIT cells increase the expression of key glycolytic enzymes (including HKII and LDH), supporting MAIT cell engagement of glycolytic metabolism upon activation. Furthermore, inhibition of MYC resulted in diminished HKII expression and rates of glycolytic metabolism, confirming that, as in conventional T cells, MYC is a key metabolic regulator. In conventional $CD8^+$ T cells, glucose metabolism is also critical for cell growth and proliferation (*46*). Here, we demonstrated that glucose metabolism and glycolysis are needed for optimal MAIT cell proliferation. Limiting glycolysis by acutely reducing glucose availability or substituting glucose with galactose further provided evidence for glucose availability being a rate-limiting step for proliferation in MAIT cells.

MAIT cell cytokine production is defective in numerous human diseases, including cancer, obesity, and coronavirus disease 2019 (*8*, *47*, *48*). Here, we showed that MAIT cell proliferation was reduced in PWO, which is consistent with reports of defective host protection in obesity. Having demonstrated the importance of MYC and its targets for MAIT cell proliferation, we investigated the impact of obesity on MYC and observed reduced MYC activity in MAIT cells from PWO. Furthermore, we highlight that this is not due to reduced MYC mRNA expression in immune-activated MAIT cells from PWO. MYC protein has a short half-life because of constant proteasomal degradation. Increased MYC protein levels are thus only seen in cells with sufficient amino acid transport capable of fueling protein synthesis in a self-fulfilling feed-forward loop (*24*–*26*, *49*, *50*). We noted that expression of key MYC targets such as SLC7A5 were also defective in MAIT cells isolated from PWO, as would be expected with impaired MYC-driven transcription. We have previously demonstrated that defects in glucose metabolism in both MAIT cells and NK cells from PWO underlie blunted cytokine production of these cells (*27*–*29*). The identification of defective MYC expression in MAIT cells from PWO helps to further understand these observations.

In conclusion, we have identified MYC as a regulator of MAIT cell metabolism. We demonstrate that a MYC-SLC7A5-glycolysis axis is needed for MAIT cell proliferation and that this is defective in obesity. However, these data extend beyond obesity and provide insight into the molecular and metabolic regulation of MAIT cell proliferation, which will have particular relevance for the potential use of MAIT cells for immunotherapy (*21*).

## MATERIALS AND METHODS

### Study cohorts and ethical approval

A total cohort of 50 adults (25 obese and 25 nonobese) were recruited. Inclusion criteria included ability to give informed consent, 18 to 65 years of age, and a body mass index (BMI) < 28 for the nonobese control cohort and BMI > 30 for the obese cohort. Exclusion

criteria for both cohorts included having a current or recent (<2 weeks) infection, being a current smoker, and using anti-inflammatory medications, including glucagon-like peptide-1 (GLP-1) analog therapies. Ethical approval was obtained from both the St. Vincent's University Medical Ethics Committee and the Maynooth University Ethics Committee.

### Preparation of peripheral blood mononuclear cells and flow cytometric analysis

Peripheral blood mononuclear cell (PBMC) samples were isolated by density centrifugation over Ficoll from fresh peripheral blood samples. MAIT cell staining was performed using specific surface monoclonal antibodies (all Miltenyi Biotec), namely, CD3 (REA613), CD161 (REA631), CD8 (REA734), and TCRVα7.2 (REA179) (fig. S7) in addition to CD25 (REA570), CD71 (REA902), and CD98 (REA387). Cell populations were acquired using an Attune NXT flow cytometer and analyzed using FlowJo software (Treestar). Results are expressed as a percentage of the parent population, as indicated and determined using flow minus-1 (FMO) and unstained controls.

### MAIT cell proliferation analysis

Fresh PBMCs ($1 \times 10^6$/ml) were stimulated for 18 hours with 5-ARU (1 μg/ml) and 100 μM methylglyoxal in the absence or presence of specific metabolic inhibitors [2-DG (2 mM), 10074-G5 (10 μM), iBET762 (10 μM), or BCH (50 mM)]. After 18 hours, RPMI 1640 was replaced with fresh culture media containing IL-2 (33.3 ng/ml). Cultures were maintained for up to 28 days, replacing the media with fresh culture media containing IL-2 every 3 days. MAIT cell proliferation was determined by either flow cytometric analysis of MAIT cell frequencies or CellTrace Violet (CTV) proliferation assays.

### MAIT cell proteomic sample preparation

Purified IL-2–expanded MAIT cells ($MAIT^{IL\text{-}2}$) were stimulated for 18 hours with anti-CD3/CD28 Dynabeads (Thermo Fisher Scientific) as well as IL-12 (50 ng/ml) and IL-18 (50 ng/ml) for 18 hours. Cell pellets were lysed at room temperature in 5% SDS, 50 mM TEAB (pH 8.5), and 10 mM TCEP under agitation for 30 min, then boiled for 5 min, and sonicated with a BioRuptor (30-s on, 30-s off × 15 cycles). Protein concentration was determined using an EZQ protein quantification kit (Invitrogen) according to the manufacturer's protocol. Lysates were alkylated with 20 mM iodoacetamide for 1 hour at room temperature in the dark. The samples were then processed using S-Trap micro columns (Protifi). Aqueous phosphoric acid (12%) was added at 1:10 to each sample for a final concentration of ~1.2% phosphoric acid. Samples were transferred to 5 ml–lo-bind microcentrifuge tubes (Eppendorf). S-Trap binding buffer [3200 μl; 100 mM TEAB (pH 7.1) adjusted using phosphoric acid and 90% MeOH] was added to each sample. Each sample was loaded onto an S-Trap column in batches of 165 μl and centrifuged at 4000*g* for 30 s or until all SDS lysate/S-Trap buffer had passed through the S-Trap column. Loading and centrifuging of columns was repeated until all the lysates were run through the column. The captured protein was then washed by adding 150 μl of S-Trap binding buffer to columns, which were then spun at 4000*g* for 30 s: Columns were washed five times in total. Columns were transferred to fresh 2-ml collection tubes. Twenty microliters of digestion buffer [50 mM ammonium bicarbonate in high-performance liquid chromatography (HPLC) water] containing 1:20 trypsin were added onto each column. Samples were centrifuged at 4000*g* for 30 s, and any solution that passed through was returned to the top of the column. Tubes were incubated for 2 hours at 47°C. Forty microliters of digestion buffer containing trypsin were added to each column. Samples were centrifuged at 1000*g* for 60 s, and the peptide elution was kept. Forty microliters of 0.2% aqueous formic acid were added to the S-Trap protein-trapping matrix and centrifuged at 1000*g* for 60 s into the same collection tube. Forty microliters of 50% aqueous acetonitrile containing 0.2% formic acid were added, and samples were centrifuged at 4000*g* for 60 s for a final elution.

### Data-independent acquisition MS acquisition

An equivalent of 1.5-μg peptides was injected onto a nanoscale C18 reverse-phase chromatography column coupled to an UltiMate 3000 RSLC nano HPLC system (Thermo Fisher Science) and an Orbitrap Exploris 480 mass spectrometer (Thermo Fisher Scientific). For liquid chromatography, the following buffers were used: buffer A [0.1% formic acid in Milli-Q water (v/v)] and buffer B [80% acetonitrile and 0.1% formic acid in Milli-Q water (v/v)]. Samples were loaded at 10 μl/min onto a trap column (100 μm by 2 cm, PepMap NanoViper C18 column, 5 μm, 100 Å; Thermo Fisher Scientific) equilibrated in 0.1% trifluoroacetic acid (TFA). The trap column was washed for 3 min at the same flow rate with 0.1% TFA and then switched in-line with a Thermo Fisher Scientific resolving C18 column (75 μm by 50 cm, PepMap RSLC C18 column, 2 μm, 100 Å). Peptides were eluted from the column at a constant flow rate of 300 nl/min with a linear gradient from 3 to 6% buffer B in 5 min, then from 6 to 35% buffer B in 115 min, and lastly to 80% buffer B within 7 min. The column was then washed with 80% buffer B for 4 min and re-equilibrated in 3% buffer B for 15 min. Two blanks were run between each sample to reduce carryover. The column was kept at a constant temperature of 50°C.

The data were acquired using an easy spray source operated in positive mode with spray voltage at 2.6 kV, and the ion transfer tube temperature was at 250°C. The MS was operated in data-independent acquisition (DIA) mode. A scan cycle comprised a full MS scan (mass/charge ratio range from 350 to 1650), with RF lens at 40%, AGC target set to custom, normalized AGC target at 300%, maximum injection time mode set to custom, maximum injection time at 20 ms, microscan set to 1, and source fragmentation disabled. MS survey scan was followed by tandem MS (MS/MS) DIA scan events using the following parameters: multiplex ions set to false; collision energy mode set to stepped; collision energy type set to normalized; HCD collision energies set to 25.5, 27, and 30%; orbitrap resolution of 30,000; first mass of 200; RF lens at 40%; AGC target set to custom; normalized AGC target of 3000%; microscan set to 1; and maximum injection time of 55 ms. Data for both MS scan and MS/MS DIA scan events were acquired in profile mode. The method used for the DIA MS was based on a previously published approach (*51*).

### DIA data quantification and analysis

Quantification of reporter ions was completed using Spectronaut (VX, Biognosys; Spectronaut 15.2.210819.50606) in library-free (directDIA) mode. Minimum peptide length was set to 7, and maximum peptide length was set to 52, with a maximum of 2 missed cleavages. MS1 and MS2 mass tolerance strategy and XIC

IM and RT extraction windows were set to dynamic, all with a correction factor of 1. Trypsin was specified as the digestive enzyme used. The false discovery rate (FDR) at the precursor ion level and protein level was set at 1% (protein and precursor *Q* value cutoff). The max number of variable modifications was set to 5, with protein N-terminal acetylation and glutamine and asparagine deamidation set as variable modifications. Carbamidomethylation of cysteine residues was selected as a fixed modification. For calibration, the MS1 and MS2 mass tolerance strategy was set to the system default. Machine learning was set across experiments, with a precursor PEP cutoff of 0.2 and a protein *Q* value cutoff of 0.01. Single-hit proteins were not excluded, with single hits defined by stripped sequence. For quantification, the quantification method was set to QUANT 2.0. Inference correction was set to true, with MS1 min of 2 and MS2 min of 3. The major protein grouping was by protein group ID, and the minor peptide grouping was set to stripped sequence. Major and minor group top *N* was set to false, with minor and major group quantities set to sum precursor quantity and sum peptide quantity, respectively. Quantity at the MS level was set to MS2, and quantity type was set to area. Proteotypicity filter was set to none, data filtering to *Q* value, and cross run normalization was switched off. MS2 demultiplexing was automatic, and the run limit for the directDIA library was set to −1, with no profiling strategy or unify peptide peaks strategy. Data filtering and protein copy number quantification were performed in the Perseus software package, version 1.6.6.0. Copy numbers were calculated using the proteomic ruler (*30*). This method sets the summed peptide intensities of the histones to the number of histones in a typical diploid cell. The ratio between the histone peptide intensity and summed peptide intensities of all other identified proteins is then used to estimate the protein copy number per cell for all the identified proteins. Further filtration of the data was completed to include proteins detected in at least two biological replicates and to exclude proteins identified on the basis of single peptides.

### CTV proliferation assay

MAIT cell proliferation was also measured using a CTV proliferation kit (Thermo Fisher Scientific) according to the manufacturer's instructions. Briefly, CellTrace solution was prepared immediately before use to 5 mM stock using dimethyl sulfoxide. Next, the dye was diluted to 5 μM working concentration by adding an appropriate amount of the stock solution into prewarmed phosphate-buffered saline (PBS). Isolated PBMCs were stained at $10^6$ cells per ml of the PBS-dye solution. Cells were incubated for 20 min at room temperature and protected from light with circular agitation. Unbound dye was washed away with RPMI 1640, and cells were incubated for at least 10 min to allow acetate hydrolysis of the dye. CTV-stained cells were stimulated for 18 hours with 5-ARU (1 μg/ml) and 100 μM methylglyoxal in the absence or presence of specific metabolic inhibitors [2-DG (2 mM), 10074-G5 (10 μM), iBET762 (25 nM), or BCH (50 mM)]. After 18 hours, the media was replaced with fresh culture media containing IL-2 (33.3 ng/ml). Cultures were maintained for 5 days before analysis.

### MAIT cell metabolic analysis

Fresh PBMCs ($1 \times 10^6$/ml) or $MAIT^{IL\text{-}2}$ cells were activated using Dynabeads, IL-12 (50 ng/ml), and IL-18 (50 ng/ml) for 18 hours. Cells were then labeled for extracellular markers, fixed, and permeabilized using the True-Nuclear transcription factor buffer set (BioLegend) according to the manufacturer's instructions before intracellular staining with monoclonal antibodies specific for HKII (Abcam, EPR20839), LDH (Abcam, EP1563Y), or MYC (Cell Signaling Technology, D84C12).

### MAIT cell Seahorse experiments

For real-time analysis of the extracellular acidification rate (ECAR), $MAIT^{IL\text{-}2}$ cells were cultured in the absence or presence of stimulation [Dynabead as well as IL-12 and IL-18 (both 50 ng/ml)] and the MYC inhibitor iBET762 (25 mM) for 18 hours before analysis on a Seahorse XF-96 analyzer (Seahorse Bioscience). Briefly, 200,000 MAIT cells were adhered to a CellTaq (BD Pharmingen)–coated 96-well XF cell culture microplate (Seahorse Biosciences). Sequential measurements of ECAR after addition of the inhibitors (Sigma-Aldrich) oligomycin (2 μM) and 2-DG (30 mM) allowed for the calculation of basal glycolysis. Each cell culture condition was evaluated in quadruplicate, and 14 measurements were made per sample.

### MAIT cell kynurenine and BCH experiments

MAIT cells activated for 18 hours (Dynabeads and IL-12/IL-18, both 50 ng/ml) in the absence or presence of a MYC inhibitor (iBET 762, 25 nM) were washed and resuspended in 200 ml of warmed Hank's balanced salt solution (HBSS) ($1 \times 10^6$ cells) and incubated in a water bath at 37°C. Kynurenine (200 mM, in HBSS) was warmed to 37°C, with a 4°C control, and added as appropriate. Uptake was stopped after 4 min by paraformaldehyde (final concentration of 1%) for 30 min at room temperature in the dark. After fixation, cells were washed twice in PBS/0.5% bovine serum albumin (BSA) and resuspended in PBS/0.5% BSA before acquisition on a flow cytometer. The 405-nm laser and 450/50 band pass (BP) filter were used for kynurenine fluorescence detection. For SLC7A5 inhibition experiments, the concentration of amino acids in RPMI was diluted twofold using HBSS (Invitrogen) in the presence or absence of BCH (50 mM; Sigma-Aldrich).

### Polymerase chain reaction gene expression

mRNA was extracted from MAIT cells from healthy controls and PWO using the EZNA total RNA kit I (Omega Bio-tek) according to the manufacturer's protocol. Synthesis of cDNA was performed using the qScript cDNA Synthesis kit (QuantaBio). Real-time reverse transcription quantitative polymerase chain reaction was performed using the PerfeCTa SYBR Green FastMix Reaction Mix (Green Fastmix, ROX) (QuantaBio) and KiCqStart primer sets (Sigma-Aldrich).

### Western blotting analysis

Human $MAIT^{IL\text{-}2}$ cells ($2.5 \times 10^6$) were cultured in 24-well plates stimulated with various stimuli [Dynabeads, IL-2 (10 to 40 ng/ml), IL-12 (50 ng/ml), and IL-18 (50 ng/ml)] for 18 hours [in the absence or presence of STAT5 inhibitor (CAS 285986-31-4, Merck)] before harvesting for Western blotting. Cells were lysed in NP-40 lysis buffer [50 mM tris-HCI (pH 7.4) containing 150 mM NaCl, 1% (w/v) IGEPAL (Sigma-Aldrich), and complete protease inhibitor mixture (Roche)]. Samples were resolved using SDS–polyacrylamide gel electrophoresis and transferred to nitrocellulose membranes before analysis with anti-MYC (Cell Signaling Technology) and anti–β-actin (Sigma-Aldrich) antibodies. Protein bands were visualized using enhanced chemiluminescence.

### In silico RNA sequencing analysis

Publicly available RNA sequencing data sets of MAIT cells were downloaded from Gene Expression Omnibus (GEO) accession number GSE123805 (*11*) and National Center for Biotechnology Information (NCBI) Sequence Read Archive (SRA) accession number PRJNA559574 (*10*). Raw read counts were downloaded from GEO (*11*), and the data analysis pipeline to this point is detailed in the associated paper. Moreover, raw sequencing data in the format of FASTQ files were downloaded from the NCBI SRA (*10*), and the following data analysis pipeline was implemented. The TrimGalore (v0.6.6) tool was used with Cutadapt (v1.15) and FastQC to apply quality and adapter trimming to FASTQ files. STAR (v2.7.9a) was used to align trimmed reads to the human genome (*Homo sapiens* high-coverage assembly GRCh38 from the Genome Reference Consortium, GRCh38.p13) with the quantMode GeneCounts option to output read counts per gene. The Bioconductor package EdgeR (v3.28.1) was applied in R (v3.6.3) to identify statistically significant differentially expressed genes between patient groups. Biological and technical variation was accounted for by the negative binomial distribution of RNA sequencing count data using a generalization of the Poisson distribution model. The filterByExpr function was applied to remove lowly expressed genes. The data were normalized across library sizes and between samples using the trimmed mean of *M* values normalization method. Tagwise dispersions were estimated for the normalized dataset. *P* values from multiple comparisons were corrected with the Benjamini-Hochberg method in EdgeR. For the comparisons between stimulations and controls, genes were considered significantly differentially expressed with an FDR-adjusted *P* value of <0.1. The Variance Modeling at the Observational Level (VOOM) method within edgeR was used to output normalized read counts as LogCPM values. These were used to perform hierarchical clustering and to construct heatmaps in Gene Pattern's online server (v3.9.11) and to perform GSEA (v4.1.0) with annotated Hallmark gene sets from the MSigDB (Molecular Signatures Database) collections (v6.2). Venn diagrams were constructed using InteractiVenn (*52*).

### Statistics

Statistical analysis was completed using Graph Pad Prism 6 Software (USA). Data are expressed as SEM. We determined differences between two groups using Student's *t* test and Mann-Whitney *U* test, where appropriate. Analysis across three or more groups was performed using analysis of variance (ANOVA). Correlations were determined using linear regression models and were expressed using Pearson or Spearman's rank correlation coefficient, as appropriate. *P* values are expressed with significance set at <0.05.

## Supplementary Materials

**This PDF file includes:**
Figs. S1 to S7

**Other Supplementary Material for this manuscript includes the following:**
MDAR Reproducibility Checklist
Data file S1

View/request a protocol for this paper from *Bio-protocol*.

## REFERENCES AND NOTES


1. D. I. Godfrey, H.-F. Koay, J. McCluskey, N. A. Gherardin, The biology and functional importance of MAIT cells. *Nat. Immunol.* **20**, 1110–1128 (2019).
2. L. Le Bourhis, E. Martin, I. Péguillet, A. Guihot, N. Froux, M. Coré, E. Lévy, M. Dusseaux, V. Meyssonnier, V. Premel, C. Ngo, B. Riteau, L. Duban, D. Robert, S. Huang, M. Rottman, C. Soudais, O. Lantz, Antimicrobial activity of mucosal-associated invariant T cells. *Nat. Immunol.* **11**, 701–708 (2010).
3. B. van Wilgenburg, I. Scherwitzl, E. C. Hutchinson, T. Leng, A. Kurioka, C. Kulicke, C. de Lara, S. Cole, S. Vasanawathana, W. Limpitikul, P. Malasit, D. Young, L. Denney; STOP-HCV consortium, E. Barnes, J. Ball, G. Burgess, G. Cooke, J. Dillon, C. Gore, G. Foster, N. Guha, R. Halford, C. Herath, C. Holmes, A. Howe, E. Hudson, W. Irving, S. Khakoo, D. Koletzki, N. Martin, T. Mbisa, J. McKeating, J. McLauchlan, A. Miners, A. Murray, P. Shaw, P. Simmonds, C. Spencer, P. Targett-Adams, E. Thomson, P. Vickerman, N. Zitzmann, M. D. Moore, P. Fabris, M. T. Giordani, Y. H. Oo, S. M. Laidlaw, L. B. Dustin, L. P. Ho, F. M. Thompson, N. Ramamurthy, J. Mongkolsapaya, C. B. Willberg, G. R. Screaton, P. Klenerman, MAIT cells are activated during human viral infections. *Nat. Commun.* **7**, 11653 (2016).
4. E. Treiner, L. Duban, S. Bahram, M. Radosavljevic, V. Wanner, F. Tilloy, P. Affaticati, S. Gilfillan, O. Lantz, Selection of evolutionarily conserved mucosal-associated invariant T cells by MR1. *Nature* **422**, 164–169 (2003).
5. L. Kjer-Nielsen, O. Patel, A. J. Corbett, J. le Nours, B. Meehan, L. Liu, M. Bhati, Z. Chen, L. Kostenko, R. Reantragoon, N. A. Williamson, A. W. Purcell, N. L. Dudek, M. J. McConville, R. A. J. O'Hair, G. N. Khairallah, D. I. Godfrey, D. P. Fairlie, J. Rossjohn, J. McCluskey, MR1 presents microbial vitamin B metabolites to MAIT cells. *Nature* **491**, 717–723 (2012).
6. N. M. Provine, P. Klenerman, MAIT cells in health and disease. *Annu. Rev. Immunol.* **38**, 203–228 (2020).
7. L. Gapin, Check MAIT. *J. Immunol.* **192**, 4475–4480 (2014).
8. C. O'Neill, F. C. Cassidy, D. O'Shea, A. E. Hogan, Mucosal associated invariant t cells in cancer-friend or foe? *Cancers (Basel)* **13**, 1582 (2021).
9. T. Leng, H. D. Akther, C.-P. Hackstein, K. Powell, T. King, M. Friedrich, Z. Christoforidou, S. McCuaig, M. Neyazi, C. V. Arancibia-Cárcamo, J. Hagel, F. Powrie; Oxford IBD Investigators, R. S. Peres, V. Millar, D. Ebner, R. Lamichhane, J. Ussher, T. S. C. Hinks, E. Marchi, C. Willberg, P. Klenerman, TCR and inflammatory signals tune human MAIT cells to exert specific tissue repair and effector functions. *Cell Rep.* **28**, 3077–3091.e5 (2019).
10. R. Lamichhane, M. Schneider, S. M. de la Harpe, T. W. R. Harrop, R. F. Hannaway, P. K. Dearden, J. R. Kirman, J. D. A. Tyndall, A. J. Vernall, J. E. Ussher, TCR- or cytokine-activated $CD8^+$ mucosal-associated invariant T cells are rapid polyfunctional effectors that can coordinate immune responses. *Cell Rep.* **28**, 3061–3076.e5 (2019).
11. T. S. C. Hinks, E. Marchi, M. Jabeen, M. Olshansky, A. Kurioka, T. J. Pediongco, B. S. Meehan, L. Kostenko, S. J. Turner, A. J. Corbett, Z. Chen, P. Klenerman, J. McCluskey, Activation and in vivo evolution of the MAIT cell transcriptome in mice and humans reveals tissue repair functionality. *Cell Rep.* **28**, 3249–3262.e5 (2019).
12. C. K. Slichter, A. McDavid, H. W. Miller, G. Finak, B. J. Seymour, J. P. McNevin, G. Diaz, J. L. Czartoski, M. J. McElrath, R. Gottardo, M. Prlic, Distinct activation thresholds of human conventional and innate-like memory T cells. *JCI Insight* **1**, e86292 (2016).
13. A. Chiba, R. Tajima, C. Tomi, Y. Miyazaki, T. Yamamura, S. Miyake, Mucosal-associated invariant T cells promote inflammation and exacerbate disease in murine models of arthritis. *Arthritis Rheum.* **64**, 153–161 (2012).
14. E. Carolan, L. M. Tobin, B. A. Mangan, M. Corrigan, G. Gaoatswe, G. Byrne, J. Geoghegan, D. Cody, J. O'Connell, D. C. Winter, D. G. Doherty, L. Lynch, D. O'Shea, A. E. Hogan, Altered distribution and increased IL-17 production by mucosal-associated invariant T cells in adult and childhood obesity. *J. Immunol.* **194**, 5775–5780 (2015).
15. C. Cosgrove, J. E. Ussher, A. Rauch, K. Gärtner, A. Kurioka, M. H. Hühn, K. Adelmann, Y.-H. Kang, J. R. Fergusson, P. Simmonds, P. Goulder, T. H. Hansen, J. Fox, H. F. Günthard, N. Khanna, F. Powrie, A. Steel, B. Gazzard, R. E. Phillips, J. Frater, H. Uhlig, P. Klenerman, Early and nonreversible decrease of CD161++ /MAIT cells in HIV infection. *Blood* **121**, 951–961 (2013).
16. E. Leeansyah, A. Ganesh, M. F. Quigley, A. Sönnerborg, J. Andersson, P. W. Hunt, M. Somsouk, S. G. Deeks, J. N. Martin, M. Moll, B. L. Shacklett, J. K. Sandberg, Activation, exhaustion, and persistent decline of the antimicrobial MR1-restricted MAIT-cell population in chronic HIV-1 infection. *Blood* **121**, 1124–1135 (2013).
17. S. J. Kang, H. M. Jin, E. J. Won, Y. N. Cho, H. J. Jung, Y. S. Kwon, H. J. Kee, J. K. Ju, J. C. Kim, U. J. Kim, H. C. Jang, S. I. Jung, S. J. Kee, Y. W. Park, Activation, impaired tumor necrosis factor-α production, and deficiency of circulating mucosal-associated invariant T cells in patients with scrub typhus. *PLOS Negl. Trop. Dis.* **10**, e0004832 (2016).
18. R. Bergin, D. Kinlen, N. Kedia-Mehta, E. Hayes, F. C. Cassidy, D. Cody, D. O'Shea, A. E. Hogan, Mucosal-associated invariant T cells are associated with insulin resistance in childhood obesity, and disrupt insulin signalling via IL-17. *Diabetologia* **65**, 1012–1017 (2022).
19. M. Gutierrez-Arcelus, N. Teslovich, A. R. Mola, R. B. Polidoro, A. Nathan, H. Kim, S. Hannes, K. Slowikowski, G. F. M. Watts, I. Korsunsky, M. B. Brenner, S. Raychaudhuri, P. J. Brennan,

Lymphocyte innateness defined by transcriptional states reflects a balance between proliferation and effector functions. *Nat. Commun.* **10**, 687 (2019).
20. L. J. Howson, G. Napolitani, D. Shepherd, H. Ghadbane, P. Kurupati, L. Preciado-Llanes, M. Rei, H. C. Dobinson, M. M. Gibani, K. W. W. Teng, E. W. Newell, N. Veerapen, G. S. Besra, A. J. Pollard, V. Cerundolo, MAIT cell clonal expansion and TCR repertoire shaping in human volunteers challenged with Salmonella Paratyphi A. *Nat. Commun.* **9**, 253 (2018).
21. T. Parrot, K. Healy, C. Boulouis, M. J. Sobkowiak, E. Leeansyah, S. Aleman, A. Bertoletti, M. S. Chen, J. K. Sandberg, Expansion of donor-unrestricted MAIT cells with enhanced cytolytic function suitable for TCR redirection. *JCI Insight* **6**, e140074 (2021).
22. E. A. Newsholme, B. Crabtree, M. S. Ardawi, The role of high rates of glycolysis and glutamine utilization in rapidly dividing cells. *Biosci. Rep.* **5**, 393–400 (1985).
23. R. Wang, C. P. Dillon, L. Z. Shi, S. Milasta, R. Carter, D. Finkelstein, L. L. McCormick, P. Fitzgerald, H. Chi, J. Munger, D. R. Green, The transcription factor Myc controls metabolic reprogramming upon T lymphocyte activation. *Immunity* **35**, 871–882 (2011).
24. J. M. Marchingo, L. V. Sinclair, A. J. Howden, D. A. Cantrell, Quantitative analysis of how Myc controls T cell proteomes and metabolic pathways during T cell activation. *eLife* **9**, e53725 (2020).
25. L. V. Sinclair, J. Rolf, E. Emslie, Y.-B. Shi, P. M. Taylor, D. A. Cantrell, Control of amino-acid transport by antigen receptors coordinates the metabolic reprogramming essential for T cell differentiation. *Nat. Immunol.* **14**, 500–508 (2013).
26. G. C. Preston, L. V. Sinclair, A. Kaskar, J. L. Hukelmann, M. N. Navarro, I. Ferrero, H. R. MacDonald, V. H. Cowling, D. A. Cantrell, Single cell tuning of Myc expression by antigen receptor signal strength and interleukin-2 in T lymphocytes. *EMBO J.* **34**, 2008–2024 (2015).
27. A. O'Brien, R. M. Loftus, M. M. Pisarska, L. M. Tobin, R. Bergin, N. A. W. Wood, C. Foley, A. Mat, F. C. Tinley, C. Bannan, G. Sommerville, N. Veerapen, G. S. Besra, L. V. Sinclair, P. N. Moynagh, L. Lynch, D. K. Finlay, D. O'Shea, A. E. Hogan, Obesity reduces mTORC1 activity in mucosal-associated invariant T cells, driving defective metabolic and functional responses. *J. Immunol.* **202**, 3404–3411 (2019).
28. L. M. Tobin, M. Mavinkurve, E. Carolan, D. Kinlen, E. C. O'Brien, M. A. Little, D. K. Finlay, D. Cody, A. E. Hogan, D. O'Shea, NK cells in childhood obesity are activated, metabolically stressed, and functionally deficient. *JCI Insight* **2**, e94939 (2017).
29. X. Michelet, L. Dyck, A. Hogan, R. M. Loftus, D. Duquette, K. Wei, S. Beyaz, A. Tavakkoli, C. Foley, R. Donnelly, C. O'Farrelly, M. Raverdeau, A. Vernon, W. Pettee, D. O'Shea, B. S. Nikolajczyk, K. H. G. Mills, M. B. Brenner, D. Finlay, L. Lynch, Metabolic reprogramming of natural killer cells in obesity limits antitumor responses. *Nat. Immunol.* **19**, 1330–1340 (2018).
30. J. R. Wisniewski, M. Y. Hein, J. Cox, M. Mann, A "proteomic ruler" for protein copy number and concentration estimation without spike-in standards. *Mol. Cell. Proteomics* **13**, 3497–3506 (2014).
31. A. J. M. Howden, J. L. Hukelmann, A. Brenes, L. Spinelli, L. V. Sinclair, A. I. Lamond, D. A. Cantrell, Quantitative analysis of T cell proteomes and environmental sensors during T cell differentiation. *Nat. Immunol.* **20**, 1542–1554 (2019).
32. J. L. Hukelmann, K. E. Anderson, L. V. Sinclair, K. M. Grzes, A. B. Murillo, P. T. Hawkins, L. R. Stephens, A. I. Lamond, D. A. Cantrell, The cytotoxic T cell proteome and its shaping by the kinase mTOR. *Nat. Immunol.* **17**, 104–112 (2016).
33. G. H. Cornish, L. V. Sinclair, D. A. Cantrell, Differential regulation of T-cell growth by IL-2 and IL-15. *Blood* **108**, 600–608 (2006).
34. B. Amati, M. W. Brooks, N. Levy, T. D. Littlewood, G. I. Evan, H. Land, Oncogenic activity of the c-Myc protein requires dimerization with Max. *Cell* **72**, 233–245 (1993).
35. J. L. Yap, H. Wang, A. Hu, J. Chauhan, K.-Y. Jung, R. B. Gharavi, E. V. Prochownik, S. Fletcher, Pharmacophore identification of c-Myc inhibitor 10074-G5. *Bioorg. Med. Chem. Lett.* **23**, 370–374 (2013).
36. D. Grimm, L. Altamirano, S. Paudel, L. Welker, M. E. Konkle, N. Chakraborty, M. A. Menze, Modulation of cellular energetics by galactose and pioglitazone. *Cell Tissue Res.* **369**, 641–646 (2017).
37. A. O. Brien, N. Kedia-Mehta, L. Tobin, N. Veerapen, G. S. Besra, D. O' Shea, A. E. Hogan, Targeting mitochondrial dysfunction in MAIT cells limits IL-17 production in obesity. *Cell. Mol. Immunol.* **17**, 1193–1195 (2020).
38. I. Magalhaes, K. Pingris, C. Poitou, S. Bessoles, N. Venteclef, B. Kiaf, L. Beaudoin, J. da Silva, O. Allatif, J. Rossjohn, L. Kjer-Nielsen, J. McCluskey, S. Ledoux, L. Genser, A. Torcivia, C. Soudais, O. Lantz, C. Boitard, J. Aron-Wisnewsky, E. Larger, K. Clément, A. Lehuen, Mucosal-associated invariant T cell alterations in obese and type 2 diabetic patients. *J. Clin. Invest.* **125**, 1752–1762 (2015).
39. A. Toubal, I. Nel, S. Lotersztajn, A. Lehuen, Mucosal-associated invariant T cells and disease. *Nat. Rev. Immunol.* **19**, 643–657 (2019).
40. D. I. Godfrey, J. le Nours, D. M. Andrews, A. P. Uldrich, J. Rossjohn, Unconventional T cell targets for cancer immunotherapy. *Immunity* **48**, 453–473 (2018).
41. K. Schubert, I. Karkossa, J. Schor, B. Engelmann, L. M. Steinheuer, T. Bruns, U. Rolle-Kampczyk, J. Hackermüller, M. von Bergen, A multi-omics analysis of mucosal-associated-invariant t cells reveals key drivers of distinct modes of activation. *Front. Immunol.* **12**, 616967 (2021).
42. B. Bulitta, W. Zuschratter, I. Bernal, D. Bruder, F. Klawonn, M. von Bergen, H. S. P. Garritsen, L. Jänsch, Proteomic definition of human mucosal-associated invariant T cells determines their unique molecular effector phenotype. *Eur. J. Immunol.* **48**, 1336–1349 (2018).
43. W. N. D'Souza, L. Lefrançois, IL-2 is not required for the initiation of CD8 T cell cycling but sustains expansion. *J. Immunol.* **171**, 5727–5735 (2003).
44. L. A. J. O'Neill, R. J. Kishton, J. Rathmell, A guide to immunometabolism for immunologists. *Nat. Rev. Immunol.* **16**, 553–565 (2016).
45. M. E. Zinser, A. J. Highton, A. Kurioka, B. Kronsteiner, J. Hagel, T. Leng, E. Marchi, C. Phetsouphanh, C. B. Willberg, S. J. Dunachie, P. Klenerman, Human MAIT cells show metabolic quiescence with rapid glucose-dependent upregulation of granzyme B upon stimulation. *Immunol. Cell Biol.* **96**, 666–674 (2018).
46. J. Sanchez, I. Jackson, K. R. Flaherty, T. Muliaditan, A. Schurich, Divergent impact of glucose availability on human virus-specific and generically activated CD8 T cells. *Metabolites* **10**, 461 (2020).
47. I. Magalhaes, B. Kiaf, A. Lehuen, iNKT and MAIT cell alterations in diabetes. *Front. Immunol.* **6**, 341 (2015).
48. C. McCarthy, C. P. O'Donnell, N. E. W. Kelly, D. O'Shea, A. E. Hogan, COVID-19 severity and obesity: Are MAIT cells a factor? *Lancet Respir. Med.* **9**, 445–447 (2021).
49. M. Swamy, S. Pathak, K. M. Grzes, S. Damerow, L. V. Sinclair, D. M. F. van Aalten, D. A. Cantrell, Glucose and glutamine fuel protein O-GlcNAcylation to control T cell self-renewal and malignancy. *Nat. Immunol.* **17**, 712–720 (2016).
50. L. V. Sinclair, A. J. Howden, A. Brenes, L. Spinelli, J. L. Hukelmann, A. N. Macintyre, X. Liu, S. Thomson, P. M. Taylor, J. C. Rathmell, J. W. Locasale, A. I. Lamond, D. A. Cantrell, Antigen receptor control of methionine metabolism in T cells. *eLife* **8**, e44210 (2019).
51. J. Muntel, T. Gandhi, L. Verbeke, O. M. Bernhardt, T. Treiber, R. Bruderer, L. Reiter, Surpassing 10 000 identified and quantified proteins in a single run by optimizing current LC-MS instrumentation and data analysis strategy. *Mol. Omics* **15**, 348–360 (2019).
52. H. Heberle, G. V. Meirelles, F. R. da Silva, G. P. Telles, R. Minghim, InteractiVenn: A web-based tool for the analysis of sets through Venn diagrams. *BMC Bioinformatics* **16**, 169 (2015).

**Acknowledgments:** We would like to thank all the donors and patients for supporting this project. **Funding:** This study was supported by the National Children's Research Centre. N.K.-M. is supported by Health Research Board (ILP-POR-2019-110). C.D.B. is supported by a fellowship from the Irish Research Council. Financial support for Attune NxT was provided to Maynooth University Department of Biology by Science Foundation Ireland (16/RI/3399). L. V. S. and the proteomic research was supported by a Wellcome Trust Principle Research Fellowship (205023/Z/16/Z) and Equipment Award to D. A. Cantrell (202950/Z/16/Z). **Author contributions:** N.K.-M., M.M.P., C.R., R.B., N.A.W.W., C.D.B., and C.O. performed the experiments and carried out analysis and approved the final manuscript as submitted. N.V. and G.B. provided MAIT cell reagents and aided in the design of MAIT cell activation experiments. C.F. performed the in silico RNA sequencing analysis. N.W.-K. and D.O. recruited patient cohorts and provided relevant clinical data. A.E.H., N.J., D.O., and L.V.S. conceptualized and designed the study, analyzed the data, drafted the manuscript, and approved the final manuscript as submitted. **Competing interests:** The authors declare that they have no competing interests. **Data and materials availability:** All data needed to evaluate the conclusions in the paper are present in the paper or the Supplementary Materials. All data are available from the corresponding authors in line with ethical approval. The mass spectrometry proteomics data have been deposited to the ProteomeXchange Consortium via the PRIDE partner repository with the dataset identifier PXD041544.

Submitted 24 January 2022
Accepted 28 March 2023
Published 18 April 2023
10.1126/scisignal.abo2709

Science Signaling

# The proliferation of human mucosal-associated invariant T cells requires a MYC-SLC7A5-glycolysis metabolic axis

Nidhi Kedia-Mehta, Marta M. Pisarska, Christina Rollings, Chloe ONeill, Conor De Barra, Cathriona Foley, Nicole A.W. Wood, Neil Wrigley-Kelly, Natacha Veerapen, Gurdyal Besra, Ronan Bergin, Nicholas Jones, Donal OShea, Linda V. Sinclair, and Andrew E. Hogan

*Sci. Signal.*, **16** (781), eabo2709.
DOI: 10.1126/scisignal.abo2709

**The master regulator of innate T cell metabolism**

Mucosal associated invariant T (MAIT) cells are a type of innate-like T cells that are enriched in adipose, gut, and liver tissue and that recognize bacterial metabolites. Upon activation, they proliferate and produce cytokines to promote host defense. Kedia-Mehta *et al.* showed that MAIT proliferation depended on MYC-associated pathways involving amino acid transport and glycolysis. Furthermore, MAIT cells from patients with obesity showed disrupted function and engagement of these pathways. These findings demonstrate that the canonical metabolic pathways found in conventional T cells are active in MAIT cells and may be relevant to the development of MAIT cell-based therapies and the study of obesity. —AEB







*Science Signaling* (ISSN ) is published by the American Association for the Advancement of Science. 1200 New York Avenue NW, Washington, DC 20005. The title *Science Signaling* is a registered trademark of AAAS.